Direct Computation of Nonlinear Soft–Tissue Deformation

Matthias Teschner	Sabine Girod	Bernd Girod
Telecommunications Lab.	Nat. Biocomputation Center	Information Systems Lab.
University of Erlangen	Stanford University	Stanford University
Germany	USA	USA

Abstract

A method for computing nonlinear soft–tissue deformation caused by simulated surgical procedures is presented. A mass–spring system is used to model patient individual soft–tissue. Instead of simulating dynamic behaviour, the introduced approach directly estimates the rest position of the system. Very fast and robust nonlinear soft–tissue deformation is computed using an optimization approach.

The multi–layer soft–tissue model considers features like skin turgor and gravity. The model takes into account the nonlinear stress–strain relationship of soft–tissue and the fact that soft–tissue is almost incompressible due to its liquid components.

The approach to soft–tissue deformation is part of an integrated system for craniofacial surgical simulation. The system is capable of simulating bone cutting and bone realignment with integrated interactive collision detection. Furthermore, soft–tissue deformation and cutting due to the application of surgical instruments can be visualized.

1 Introduction

The idea of estimating soft–tissue deformation due to bone realignment was formulated by Vannier in 1983 [26]. In 1992 further approaches to surgery simulation were introduced by Kikinis [16, 1], followed by Delingette in 1994 [8, 9, 7], Bohner in 1996 [3], Koch in 1996 [17], and Bro-Nielsen in 1998 [4]. These approaches use deformable volumes, mass–spring models, or finite elements to predict soft–tissue changes.

In this paper, a method for direct computation of soft–tissue deformation based on a mass–spring model is presented. Instead of simulating the dynamic behaviour, the introduced approach directly estimates the rest position of the system. The method is part of an integrated system for craniofacial surgical simulation [13, 14, 24, 25]. The system is capable of simulating a variety of craniofacial surgical procedures. It consists of components for simulating bone cutting and bone realignment with integrated interactive collision detection and avoidance. Nonlinear soft–tissue deformation and soft–tissue cutting can be computed using a very fast and robust optimization approach. The computation of soft–tissue deformation does not require any pre-processing time and is very efficient with regard to memory. The system handles individual patient data sets. While the model of the patient's bone structure and the patient's face is provided by a CT scan and a surface laser scan, respectively, the patient's soft–tissue is represented by a mass–spring system.

Mass–spring systems [22, 23] are not only used to model deformable soft–tissue in surgical simulation environments, but they are also widely used to model other deformable objects. They have been applied to a variety

of problems, such as cloth modeling [6, 10] and facial animation [18].

Mass–spring models assume a discretization of the object into n points $\mathbf{x_i}$ with masses m_i. These points are linked by springs and dampers. In order to compute the dynamics of a mass–spring system, the relation between position, velocity, and acceleration for point $\mathbf{x_i}$ at time t can be described by

$$m_i \frac{d^2\mathbf{x_i}(t)}{dt^2} + \gamma \frac{d\mathbf{x_i}(t)}{dt} + \mathbf{F_i^{int}}(t) = \mathbf{F_i^{ext}}(t) \quad (1)$$

with γ denoting a damping factor, $\mathbf{F_i^{int}}$ denoting the internal elastic force caused by strains of adjacent springs of $\mathbf{x_i}$ and $\mathbf{F_i^{ext}}$ denoting the sum of external forces. Thus, the dynamics of the entire object is described by a system of second-order ordinary differential equations. Eq. 1 can be reduced to two coupled first–order differential equations

$$\frac{d\mathbf{x_i}(t)}{dt} = \mathbf{v_i}(t) \quad (2)$$

$$\frac{d\mathbf{v_i}(t)}{dt} = \frac{\mathbf{F_i^{ext}}(t) - \mathbf{F_i^{int}}(t) - \gamma \mathbf{v_i}(t)}{m_i} \quad (3)$$

with $\mathbf{v_i}$ denoting the velocity of point $\mathbf{x_i}$. Given initial values for $\mathbf{x_i}$, $\mathbf{v_i}$, $\mathbf{F_i^{int}}$, and $\mathbf{F_i^{ext}}$ at time t, Euler's method is commonly applied to numerically integrate through time:

$$\mathbf{x_i}(t + \Delta t) = \mathbf{x_i}(t) + \Delta t \mathbf{v_i}(t) \quad (4)$$

$$\mathbf{v_i}(t + \Delta t) =$$
$$\mathbf{v_i}(t) + \Delta t \frac{\mathbf{F_i^{ext}}(t) - \mathbf{F_i^{int}}(t) - \gamma \mathbf{v_i}(t)}{m_i} (5)$$

This scheme can be used to compute the dynamic behavior of a deformable mass–spring model [15]. Other approaches employ higher–order Runge–Kutta methods [2] or finite differences [11].

Excellent results can be achieved by applying these methods in order to animate deformable models. However, due to numerical problems and slow convergence these approaches are not very well suited to estimate the rest position of mass–spring systems. In this paper, a new method for estimating the rest position of a deformable soft–tissue model is introduced. Instead of simulating the dynamic behavior of soft–tissue, a very fast and robust optimization approach is applied to directly estimate the deformation due to bone realignment or due to the application of surgical instruments.

The paper is organized as follows. Due to the fact, that individual patient data sets are used for soft–tissue prediction, the next section describes the generation of 3–D models of the patient's bone structure and the patient's face. In Section 3 the structure of the soft–tissue model is described. In Section 4 the approach to nonlinear soft–tissue deformation is introduced. Simulation results are presented in Section 5.

2 Data Acquisition

Triangle meshes that describe the surface of the face and the bone structure of the head are the basic models of the surgery simulation system. These meshes are built using two different sensory modalities. A computer tomography scan provides the anatomically correct representation of the bone structure and a laser scanner records a photorealistic, 3–D model of the patient's face. The triangle mesh that represents the surface of the bone structure is generated by applying the Marching–Cubes algorithm [19] to the CT scan. The triangle mesh that represents the face surface is computed from the depth and color map of the laser scan. Both modalities are registered by exploiting corresponding cephalometric landmarks of the laser scan and the skin surface taken from the CT scan [15].

The extraction of isosurfaces from the CT volume data set and the surface reconstruction from the Cyberware range scanner data set easily generate hundreds of thousands of triangles. In order to enable interactive visualization and handling of these triangle meshes they must be decimated. In [5] a simplification method is proposed that incor-

porates the one–sided Hausdorff distance as global error criterion. This algorithm is applied to the triangle meshes that describe the bone and the face surface. It guarantees that the deviation of the original and the decimated mesh is not larger than the given one–sided Hausdorff distance.

3   Soft–Tissue Model

The proposed approach to compute soft–tissue deformation caused by surgical procedures employs a multi–layer spring model. The soft–tissue model basically consists of three types of points, which are connected with springs. *Soft–tissue point set P* consists of soft–tissue points. A soft–tissue point $\mathbf{p} \in P$ is characterized by its position $\mathbf{p} = (x, y, z)^T$ and a mass m. *Boundary point set $P_B \subset P$* consists of boundary points which are fixed in space. The soft–tissue model is connected to several bone structures. For each bone structure i there exists a *bone point set $P_B^i \subset P$*. Bone points represent connections to a bone structure. In contrast to boundary points they are not fixed in space, but can be transformed by moving the corresponding bone structure. Point set P_B^* represents all bone points. Point set P_s represents all soft-tissue points, which are neither bone nor boundary points: $P_s = P \setminus (P_B \cup P_B^*)$.

All points are connected with springs. A spring sp_i is parametrized by its initial length l_i and a spring constant k_i, which describes its stiffness. All springs are categorized into sets according to their location and function. This allows to model differentiated elasto–mechanical properties of soft–tissue layers by assigning different spring constants k to each spring set.

Layer spring sets represent soft–tissue layers. The number and the thickness of soft–tissue layers are variable. Simulations have been performed with up to six layers. *Connecting–layer spring sets* and *diagonal connecting–layer spring sets* connect soft–tissue layers. All layer spring sets have the same structure as the triangulated skin surface. The connecting–layer springs form prismatic volume elements. Spring set S represents all springs of the model.

All point sets and spring sets are illustrated in Fig. 1.
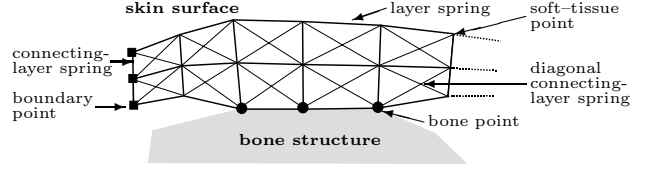
Figure 1: Three–layer soft–tissue model.

All springs in a spring set are parametrized by a spring constant k in order to model the elasto–mechanical properties of the corresponding soft–tissue layer.

The spring set that represents the skin surface can be initialized with an initial strain. This strain corresponds to the so–called skin turgor. In order to enable simulation of gravity each soft–tissue point is characterized by a mass m. Each soft–tissue layer is parametrized by an overall mass, which is distributed according to the topology and geometry of the representing soft–tissue points.

Due to mass and the initial strain of the surface, there are forces at each soft–tissue point. In order to obtain a stable equilibrium of the mesh, the resulting force at each soft–tissue point has to be zero. This is achieved by determining appropriate strains for all springs, given the initial strain of springs representing the skin surface. In order to compute the stable equilibrium an optimization approach is applied.

In the left–hand image of Fig. 2 initial forces at soft–tissue positions due to skin turgor and mass are visualized using an individual patient data set. The right–hand image of Fig. 2 illustrates the forces after applying the optimization approach. All internal forces are diverted to bone points, which have a fixed position. The optimization process required approximately seven seconds on an SGI Octane, R12000.
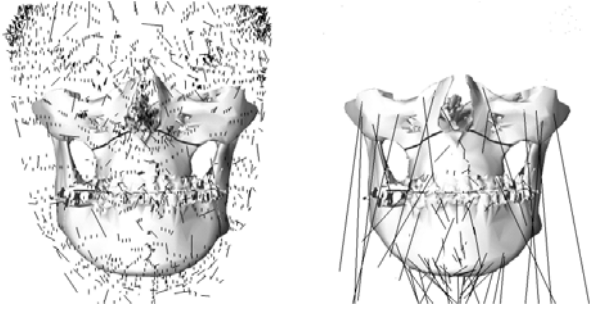
Figure 2: Forces at soft–tissue points. Left: Initial state with forces at soft–tissue points due to mass and skin turgor. Right: Stable equilibrium. Forces are diverted to bone boints which have a fixed position.

4 Nonlinear Soft–Tissue Deformation

In order to simulate soft–tissue deformation the state of the model is described by three functions. These functions are parametrized by all soft–tissue points $\mathbf{p} \in P_s$ which are neither bone nor boundary points. Function f_f (Eq. 7) describes the sum of absolute values of resulting forces $\mathbf{F_i}$ for each soft–tissue point $\mathbf{p_i} \in P_s$ with S_i denoting all springs sp_j, that are connected with $\mathbf{p_i}$ ($\mathbf{p_{1,j}} = \mathbf{p_i}$).

$$
\begin{aligned}
\mathbf{F_i} = & \sum_{j:sp_j \in S_i} k_j \left(1 - \frac{l_j}{|\mathbf{p_i} - \mathbf{p_{2,j}}|}\right) (\mathbf{p_{2,j}} - \mathbf{p_i}) \\
& + (0, 0, -m_i g)^T
\end{aligned} \tag{6}
$$

$$
f_f(P_s) = \sum_{i:\mathbf{p_i} \in P_s} |\mathbf{F_i}| \tag{7}
$$

Function f_e (Eq. 9) describes the sum of all spring energies with S denoting the set of all springs.

$$
E_i = \frac{1}{2} k_i \left(l_i - |\mathbf{p_{1,i}} - \mathbf{p_{2,i}}|\right)^2 \tag{8}
$$

$$
f_e(P_s) = \sum_{i:sp_i \in S} E_i \tag{9}
$$

Function f_v (Eq. 10) describes the difference of initial volumes $v_{0,i}$ and current volumes v_i of all prismatic volume elements. Due to lack of space the equation for estimating the volume of prismatic elements is omitted here.

$$
f_v(P_s) = \sum_i (v_{0,i} - v_i)^2 \tag{10}
$$

Functions f_f and f_v are equal to zero in the stable equilibrium of the soft–tissue model. Function f_e does not equals zero due to the fact that all springs can have a certain strain.

Soft–tissue deformation can be caused by additional external forces, which are applied to soft–tissue points, or by transforming soft–tissue points to a fixed position. Transformation of a bone structure leads to the same transformation of corresponding bone points of the soft–tissue model. Additional external forces or transformed bone points $\mathbf{p} \in P_B^*$ result in increased values for f_f, f_e, and f_v.

An optimization approach is used to estimate the deformed soft–tissue model. The optimization process is applied in order to minimize the spring mesh energy f_e (Eq. 11), or to minimize the internal forces f_f (Eq. 12). Both approaches take the volume of the soft–tissue model into account. This is due to the fact that soft–tissue is almost incompressible. The components are weighted by λ. For both approaches the multidimensional conjugate gradient method [21] is used. Tests have shown, that the conjugate gradient method provides reliable results and is very efficient with regard to memory and computational complexity [24].

$$
P_s^f = \mathrm{argmin}\left(\lambda f_f(P_s) + (1 - \lambda) f_v(P_s)\right) \tag{11}
$$
$$
P_s^e = \mathrm{argmin}\left(\lambda f_e(P_s) + (1 - \lambda) f_v(P_s)\right) \tag{12}
$$

P_s^f and P_s^e describe the soft–tissue points of the deformed soft–tissue model with minimized energy and minimized resulting forces, respectively. Experiments have shown, that energy minimization is more robust and converges faster compared with the force minimization. However, the energy minimization approach is not able to take gravity into consideration.

The functions, which are used in the optimization process, basically require the com-

putation of spring force (Eq. 6) and spring energy (Eq. 9). In the linear case the absolute value of spring force F is computed as $F = k_0 s$ with k_0 denoting the spring constant and s denoting deformation (Hooke's Law). However, it has been shown, that soft–tissue has a non-linear stress–strain relationship [12, 20].

The proposed optimization approach to compute soft–tissue deformation has been extended in order to take nonlinear stress–strain relationship into account. Instead of using a constant value k_0 to compute f_f and f_e, a function $k(s)$ is introduced, which leads to a nonlinear stress–strain relationship:

$$F = k(s)s \tag{13}$$

Fig. 3 illustrates the stress–strain relationship for
$k(s) = k_0$, $k(s) = k_0(1 + s^2)$ and $k(s) = k_0(1 + s^2)^2$. Function $k(s)$ can be chosen to model linear or nonlinear stress–strain relationship. However, $k(s)$ should always converge against k_0 for small deformation s. All experimental results shown in Section 5 have been performed with $F = k_0(1 + s^2)^2 s$, and $E = \frac{1}{2}k_0\left(\frac{1}{3}s^4 + s^2 + 1\right)s^2$.
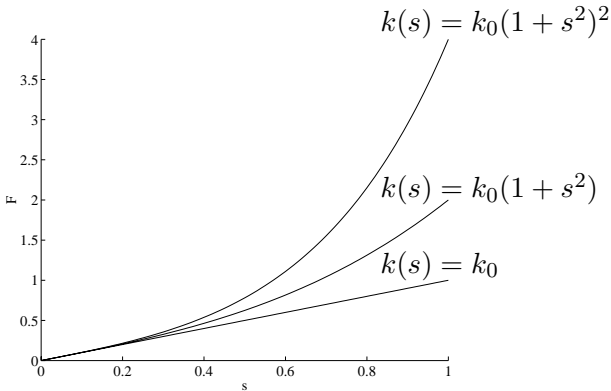
Figure 3: Nonlinear stress–strain relationship with $k_0 = 1$.

5 Results

The simulation methods for soft–tissue deformation and soft–tissue cutting have been tested with six individual patient data sets and several synthetic data sets. Fig. 4 shows the bone structure and the photo–realistic surface scan of a patient. Fig. 5 shows a physiological movement of the patient's lower jaw and the resulting soft–tissue changes. Simulations have been performed with three different soft–tissue models. Table 1 shows the parameters for the soft–tissue models which have been generated for this patient. Table 2 and Table 3 show the computation time required by the optimization process. Although the visualization of simulation results is based on SGI's OpenInventor, the soft–tissue deformation can be computed on any hardware platform, such as Sun or PC. The simulation process does not require any preprocessing time. In general, the force–based minimization process is more time consuming compared with the energy–based approach. The energy–based approach converges faster and is more robust. However, the energy minimization approach is not able to take gravity into consideration. Taking the volume preservation function into account has different effects on the minimization process. Function f_v supports the convergence in case of force–based minimization, but does not positively influence the convergence in case of energy–based minimization.

Simulation results for a second individual patient data set are shown in Fig. 6 and Fig. 7. In this case two different surgical options have been tested. Fig. 6 illustrates the original bone structure, a simulated realignment of a part of the lower jaw, and a simulated realignment of the chin. The corresponding soft–tissue prediction is shown in Fig. 7. This example illustrates the versatility of computer–based surgical planning methods compared with planning methods that use stereolithographic or milled models.

Fig. 8 illustrates the deformation of a synthetic data set caused by a synthetic surgical instrument. Some soft–tissue points are forced to a fixed position due to the synthetic surgical instrument. In addition to bone and boundary points these points are excluded from the optimization process. Thus, the position of these points is not affected by the

optimization process.

Fig. 9 illustrates soft–tissue cutting. The gap is caused by the initial strain of springs which represent the skin surface. Two simulations have been performed with different skin turgors. A soft–tissue cut is initiated due to large external forces at soft–tissue points. In this case, the topology of the soft–tissue model is modified and the optimization approach is applied. This leads to the result shown in Fig. 9.

Figure 4: Bone structure and photo–realistic surface scan of a patient.

Figure 5: Simulated jaw movement for a patient. This result has been obtained using the two–layer soft–tissue model described in Tab. 1.

Layers	Soft–tissue points	Springs	Volumes	Memory during simulation
2	954	5881	1748	2,8 MByte
4	1908	14941	2622	3,5 MByte
6	2862	24001	4370	4,3 MByte

Table 1: Parameters for three soft–tissue models generated for the patient in Fig. 4 and Fig. 5.

Layers	f_e	f_e+f_v	f_f	f_f+f_v
2	0.3	0.6	3.1	0.8
4	1.2	3.7	7.3	4.8
6	3.3	6.4	12.2	10.8

Table 2: Computation time $[s]$ for soft–tissue deformation (Fig. 5). SGI Octane, MIPS R12000, 300 MHZ, 128 MB. Functions f_f, f_e and f_v, that are used in the optimization process, are defined in Eq. 7, 9, and 10.

6 Conclusion

In this paper, a new, very efficient and robust approach to nonlinear soft–tissue deformation has been introduced. The approach takes into account the nonlinear stress–strain relationship of soft–tissue and the fact that soft–tissue is almost incompressible due to its liquid components. Mass and skin turgor are integrated in the proposed soft–tissue model.

Layers	f_e	f_e+f_v	f_f	f_f+f_v
2	0.6	1.2	4.4	1.2
4	3.2	6.3	10.4	8.1
6	8.4	14.7	19.8	17.7

Table 3: Computation time $[s]$ for soft–tissue deformation (Fig. 4). PC, Pentium III 450 MHz, 128MB. Functions f_f, f_e and f_v, that are used in the optimization process, are defined in Eq. 7, 9, and 10.

Figure 6: Simulated bone realignment. The corresponding soft–tissue changes are shown in Fig. 7.

Figure 7: Simulated soft–tissue deformation. Fig. 6 shows the corresponding bone realignment.

Instead of simulating the dynamic behaviour the approach directly computes the rest position of the deformed soft–tissue model due to surgical procedures.

Ongoing work focusses on the integration of muscles in order to simulate the patient's postoperative facial expressions. Furthermore, it is intended to perform clinical studies to estimate appropriate parameters for the introduced soft–tissue model, such as number, thickness and elasto–mechanical properties of soft–tissue layers. Postoperative surface scans, which are registered with the preoperative surface scan, will be used to compare the simulated soft–tissue deformation
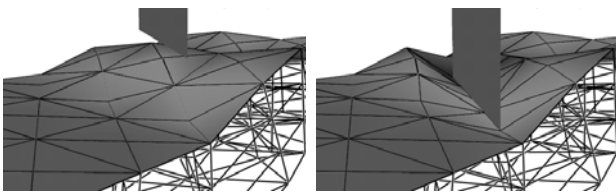
Figure 8: Simulated deformation using a synthetic data set and a synthetic surgical instrument.
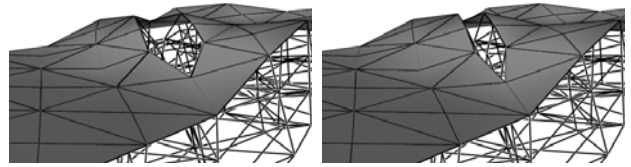
Figure 9: Simulated cutting using a synthetic data set with different values for skin turgor.

and the actual surgical result.

References

[1] D. Altobelli, R. Kikinis, J. Mulliken, H. Cline, W. Lorensen, F. Jolesz. "Computer-Assisted Three-Dimensional Planning in Craniofacial Surgery", *Journal of Oral and Maxillofacial Surgery Suppl.*, Vol. 92, 1993.

[2] D. Bielser, V. A. Maiwald, M. H. Gross. "Interactive Cuts Through 3-Dimensional Soft Tissue", *Proc. Eurographics '99, Computer Graphics Forum*, 18(3):C31–C38, 1999.

[3] P. Bohner, P. Pokrandt, S. Hassfeld. "Simultaneous Planning and Execution in Cranio-Maxillo-Facial Surgery", *Medicine Meets Virtual Reality 4 (MMVR4 '96)*, San Diego, CA, USA, 1996.

[4] M. Bro-Nielsen. "Finite Element Modeling in Surgery Simulation", *Proc. of the IEEE: Special Issue on Virtual & Augmented Reality in Medicine*, 86(3):524–530, March 1998.

[5] S. Campagna, L. Kobbelt, H.-P. Seidel. "Efficient Decimation of Complex Triangle Meshes", *University Erlangen–Nuremberg, IMMD9 Technical Report 3*, 1998.

[6] M. Carignan, Y. Yang, N. Magnenat–Thalmann, D. Thalmann. "Dressing Animated Synthetic Actors with Complex Clothes", *SIGGRAPH '92, ACM Computer Graphics*, 26(2):99–104, 1992.

[7] S. Cotin, H. Delingette, N. Ayache. "Real-Time Elastic Deformations of Soft Tissues for Surgery Simulation", *IEEE Transactions on Visualization and Computer Graphics*, 5(1):62, 1999.

[8] H. Delingette, G. Subsol, S. Cotin, J. Pignon. "A Craniofacial Surgery Simulation Testbed", *INRIA, Rapport de Recherche, Nr. 2199*, Sophia-Antipolis, 1994.

[9] H. Delingette. "Toward Realistic Soft–Tissue Modeling in Medical Simulation", *Proc. of the IEEE: Special Issue on Virtual & Augmented Reality in Medicine*, 86(3):524–530, March 1998.

[10] M. Desbrun, P. Schröder, A. Barr. "Interactive Animation of Structured Deformable Objects", In *Graphics Interface '99*, Kingston, Canada, 1999.

[11] J. Fan, Q. Wang, S.-F. Chen, M. M. F. Yuen, C. C. Chan. "A Spring–Mass Model–Based Approach for Warping Cloth Patterns on 3D Objects", *Journal of Visualization and Computer Animation*, 9:215–227, 1998.

[12] Y. C. Fung. *"Biomechanics - Mechanical Properties of Living Tissues"*, Springer, Berlin, 1993.

[13] S. Girod, E. Keeve, B. Girod. "Soft Tissue Prediction in Orthognatic Surgery by 3D CT and 3D Laser Scanning", Journal of Oral and Maxillofacial Surgery Suppl., Vol. 51, 1993.

[14] E. Keeve, S. Girod, P. Pfeifle, B. Girod. "Anatomy–Based Facial Tissue Modeling Using the Finite Element Method", In *Proc. IEEE Visualization*, San Francisco, CA, USA, 1996.

[15] E. Keeve, S. Girod, R. Kikinis, B. Girod. "Deformable Modeling of Facial Tissue for Craniofacial Surgery Simulation", *Computer Aided Surgery*, 3(5):228–238, 1998.

[16] R. Kikinis, H. Cline, D. Altobelli, M. Halle, W. Lorensen, F. Jolesz. "Interactive Visualization and Manipulation of 3D Reconstructions for the Planning of Surgical Procedures", In *Proc. Visualization in Biomedical Computing VBC '92*, pages 559–563, 1992.

[17] R. M. Koch, M. H. Gross, D. F. Bueren, G. Frankhauser, Y. Parish, F. R. Carls. "Simulating Facial Surgery Using Finite Element Models", *SIGGRAPH '96, ACM Computer Graphics*, 30, August 1996.

[18] Y. Lee, D. Terzopoulos, K. Waters. "Realistic Modeling for Facial Animation", *ACM Computer Graphics*, 29(4):55–62, 1995.

[19] W. E. Lorensen, H. E. Cline. "Marching Cubes: A High Resolution 3D Surface Construction Algorithm", *SIGGRAPH '87, ACM Computer Graphics*, 21(4):163–169, 1987.

[20] W. Maurel, Y. Wu, N. Magnenat Thalmann, D. Thalmann. *"Biomechanical Models for Soft Tissue Simulation"*, Springer, Berlin, 1998.

[21] W. Press, S. Teulolsky, W. Vetterling, B. P. Flannery. *"Numerical Recipes in C"*, Cambridge University Press, Cambridge, MA, USA, 2nd edition, 1992.

[22] D. Terzopoulos, J. Platt, A. Barr, K. Fleischer. "Elastically Deformable Models", *SIGGRAPH '87, ACM Computer Graphics*, 21(4):205–214, 1987.

[23] D. Terzopoulos, K. Fleischer. "Modeling Inelastic Deformation: Viscoelasticity, Plasticity, Fracture", *SIGGRAPH '88, ACM Computer Graphics*, 22(4):269–278, 1988.

[24] M. Teschner, S. Girod, B. Girod. "Optimization Approaches for Soft-Tissue Prediction in Craniofacial Surgery Simulation", *Proc. MICCAI '99*, pp. 1183–1190, Cambridge, England, September 1999.

[25] M. Teschner, S. Girod, B. Girod. "Surgical Planning", In *Principles of 3D Image Analysis and Synthesis*, Girod, Greiner, Niemann (ed.), Kluwer Academic Publishers, Boston, pp. 378–389, 2000.

[26] M. W. Vannier, J. L. Marsh, J. O. Warren. "Three Dimensional Computer Graphics for Craniofacial Surgical Planning and Evaluation", *SIGGRAPH '83, ACM Computer Graphics*, 17(3):263–273, 1983.